Effect of structural distortion on ferrimagnetic order in $Lu_{1-x}L_xFe_2O_4$ (L=Y and Er; x=0.0, 0.1, and 0.5)

Han-Jin Noh,* Hojin Sung, Jinwon Jeong, and Jinhwan Jeong
Department of Physics, Chonnam National University, Gwangju 500-757, Korea

Sung Baek Kim
Department of Physics, Kookmin University, Seoul 136-702, Korea

Jae-Young Kim
Pohang Accelerator Laboratory, Pohang University of Science and Technology, Pohang 790-784, Korea

J. Y. Kim and B. K. Cho
Department of Materials Science and Engineering, Gwangju Institute of Science and Technology (GIST), Gwangju 500-712, Korea
(Received 7 May 2010; revised manuscript received 17 June 2010; published 23 July 2010)

We have studied the correlation between the structural distortion and the magnetic interaction change in the ferrimagnetic $(Lu,L)Fe_2O_4$ (L=Y and Er) by using neutron powder diffraction and x-ray magnetic circular dichroism (XMCD). The Rietveld profile refinements revealed that the Y or Er substitution flattens the hexagonal unit cell of the system and asymmetrically distorts the bipyramidal FeO_5 cages with the increase in the substitution. Even in the presence of the Y or Er substitution, $\sqrt{3}\times\sqrt{3}$ superlattices are formed by Fe-valence ordering, and the interlayer magnetic coupling behavior does not change very much. Meanwhile, the Fe $2p$ XMCD spectra indicate that the Fe^{3+} spins become frustrated as the substitution increases. These results support that the unquenched orbital moment of the Fe^{2+} ions is the dominant factor for the giant magnetic anisotropy in $LuFe_2O_4$.

DOI: 10.1103/PhysRevB.82.024423 PACS number(s): 75.25.−j, 75.47.Lx, 78.70.Dm

I. INTRODUCTION

Multiferroic materials have ferroelectricity and ferromagnetism simultaneously. Traditionally, ferroelectricity is known to be established by inversion symmetry breaking through an off-center movement of transition-metal ions in d^0 insulators, so ferromagnetism which requires unpaired electrons hardly coexists with ferroelectricity in a solid.[1] However, recent studies have shown that various kinds of spin and charge orderings break inversion symmetry of a system to induce ferroelectricity.[2,3] $LuFe_2O_4$ was the first example that ferroelectricity is induced by Fe-valence ordering.[4] In $LuFe_2O_4$, the charge ordering is strongly coupled with spin degrees of freedom in a complicated manner, so the exact ordering pattern is to be a key factor to understand the underlying physics of the intriguing properties such as the giant magnetic coercivity,[5,6] magnetodielectric response,[7] and the charge fluctuation-related phenomena.[8] In particular, as to the giant magnetic coercivity, a few relevant observations were reported such as formation of pancakelike Ising domain[6,9] and a large orbital moment of the Fe^{2+} ions.[10] Further, the analysis of the x-ray magnetic circular dichroism (XMCD) spectrum at Fe $2p$ absorption edge determined a concrete spin alignment for the charge ordered phase.[10] In the spin configuration proposed in Ref. 10, the Fe^{2+} spin alignment is interpreted to be stabilized by the spin-orbit coupling of the Fe^{2+} ions while the Fe^{3+} spin alignment is done by the Fe^{3+}-O-Fe^{3+} superexchange interaction. However, the superexchange interaction is weak in the hexagonal Fe_2O_4 bilayers, so the Fe^{3+} spin alignment is expected not to be robust against an external perturbation such as site disorder or structural distortion. In this study, we introduced a site disorder and structure distortion in $LuFe_2O_4$ by substituting Y or Er ions for Lu ions, and performed neutron powder-diffraction, x-ray absorption spectroscopy (XAS), and XMCD measurements in order to testify whether the proposed mechanism is appropriate for the variation compounds.

II. EXPERIMENTALS

The polycrystalline samples of $Lu_{1-x}L_xFe_2O_4$ (L=Y and Er; x=0.0, 0.1 and 0.5) were synthesized by the standard solid-state reaction method. Stoichiometric amounts of high purity (≥99.99%) dehydrated Lu_2O_3, Y_2O_3, Er_2O_3, and Fe_3O_4 powders were weighed and mixed with a pestle and mortar. The mixtures were fired three times under $CO(20\%)/CO_2$ environment at temperature of 1200 °C for 2 days. Grinding of the materials was repeated after each firing.

The single phase of the polycrystalline samples was checked by x-ray diffraction and neutron powder diffraction. The neutron powder-diffraction experiments were performed on the high-resolution powder-diffraction neutron beam line at the HANARO research reactor, Korea. The wavelength of the monochromatized neutrons, which is achieved by a single-crystal Ge 331 surface, is 1.8345 Å. The powdered sample was loaded in a vanadium can (ϕ=10 mm, L=580 mm), and the can was placed in a helium-filled aluminum canister for the low-temperature experiments. The Rietveld profile refinements were performed by using FULLPROF.[11] Six polynomial background function, pseudo-

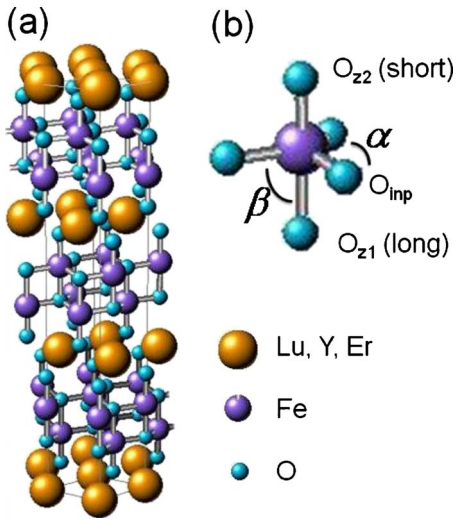

FIG. 1. (Color online) (a) Crystal structure of hexagonal bilayered $LuFe_2O_4$. (b) Bipyramidal FeO_5 cage.

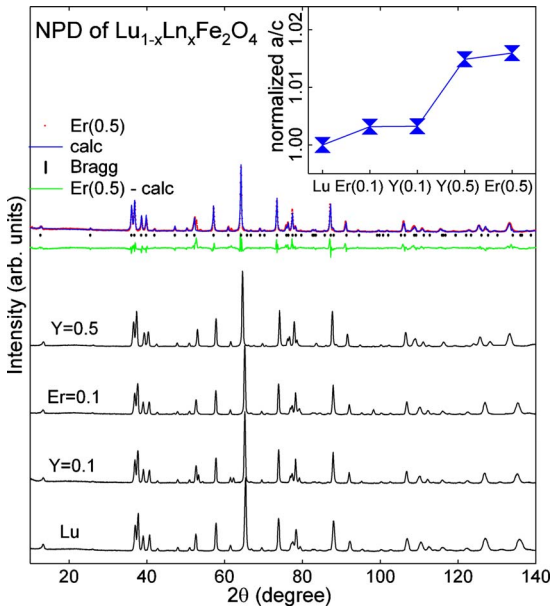

FIG. 2. (Color online) Neutron powder-diffraction patterns of hexagonal bilayered $Lu_{1-x}L_xFe_2O_4$ (L=Y and Er; x=0.0, 0.1, and 0.5) at 350 K. (Inset) Normalized a/c ratios vs L concentrations.

Voigt-type profile function with three parameters and asymmetric peak shape function with four terms were used in the refinements.

The x-ray absorption and magnetic circular dichroism experiments were performed on elliptical undulator beamline 2A at the Pohang Light Source. The samples were fractured *in situ* by the top postmethod under the pressure of $\sim 5.0 \times 10^{-10}$ Torr and at room temperature. The photon energy resolution was set to ~ 0.2 eV. All the absorption spectra were recorded in the total electron yield mode and were normalized by the incident photon flux. In the x-ray magnetic circular dichroism measurements, 98% circularly polarized photons were used. A 0.8 T electromagnet was used to align the magnetic moments at 220 K. The angle of the incident photons to the magnetic field was 22.5°.

III. RESULTS AND DISCUSSION

A. Structure analysis

The crystal structure of the mother compound $LuFe_2O_4$ is of the In_2ZnS_4 type ($R\bar{3}m$).[12] Figure 1(a) shows a conventional hexagonal unit cell for this crystal structure. It consists of a triangular Lu layer and a triangular Fe_2O_4 bilayer. The two layers are stacked up alternately along the z direction, forming three kinds of $LuFe_2O_4$ layers. The Fe_2O_4 bilayer consists of bipyramidal FeO_5 cage as shown in Fig. 1(b). The bipyramid is asymmetric. The bonding length of Fe-O_{z1} toward the other FeO_2 plane is longer than that of Fe-O_{z2} toward Lu layer. Also, the in-plane oxygen atoms do not exactly coincide with the plane of the Fe ions. As the Lu ions are substituted by Y or Er ions, the conventional unit cell is flattened, and the bipyramidal FeO_5 cage is asymmetrically distorted. These results were obtained by the Rietveld analysis of the neutron powder-diffraction patterns as shown in Fig. 2. As a result of the cell parameter change, the bonding distance between Fe and O_{inp} increases. Meanwhile, the Fe-O_{z1} bonding distance, the angle (α) of O_{inp}-Fe-O_{inp}, and the angle (β) of O_{inp}-Fe-O_{z1} decrease [see Fig. 1(b) for the notations]. These structural changes provide an important clue to understanding the XMCD spectra as will be described below. The obtained parameter values by the profile refinements are listed in Table I. In the table, the statistical error is smaller than one unit of the last digit for all the parameter values.

B. Line-shape analysis of the (1/3 1/3 *l*) superlattice peak

Below ~ 330 K, $LuFe_2O_4$ has been reported to form a $\sqrt{3} \times \sqrt{3}$ supercell in the bilayer planes[13,14] but the exact

TABLE I. Lattice constants for $Lu_{1-x}L_xFe_2O_4$ (L=Y and Er; x=0.0, 0.1 and 0.5).

System	a_0 (Å)	c_0 (Å)	Fe-O_{inp} (Å)	Fe-O_{z1} (Å)	Fe-O_{z2} (Å)	α (deg)	$180° - \beta$ (deg)
$LuFe_2O_4$	3.434	25.20	1.991	2.250	1.967	119.2	95.2
Y=0.1	3.438	25.15	1.999	2.215	1.952	118.6	96.8
Y=0.5	3.468	24.99	2.014	2.174	1.937	118.9	96.1
Er=0.1	3.441	25.17	2.002	2.222	1.943	118.4	97.2
Er=0.5	3.456	25.05	2.010	2.185	1.956	118.6	96.8

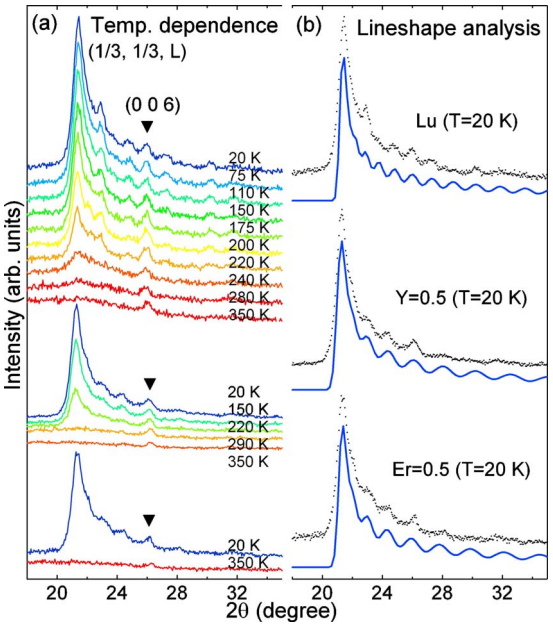

FIG. 3. (Color online) (a) Temperature dependence of the $(1/3\ 1/3\ l)$ superstructure peak in the neutron powder-diffraction patterns of $Lu_{1-x}L_xFe_2O_4$ (L=Y and Er; x=0.0 and 0.5). (b) Lineshape analysis of the $(1/3,\ 1/3,\ l)$ superstructure peak.

long-range ordering pattern along the z direction is somewhat controversial and seems to be sample dependent or oxygen stoichiometry dependent.[15–17] Although this supercell is induced by Fe-valence ordering, it is also a magnetic supercell because the spin moment of the Fe ions depends on the valence value. Thus, neutron diffraction detects this superstructure. Figure 3(a) shows the $(1/3\ 1/3\ l)$ superstructure peak in the temperature-dependent neutron powder-diffraction patterns. At temperature of 350 K, all the samples do not show the superstructure peak but with the decrease in the temperature the peak starts to appear and becomes sharp, indicating that the domain size of the superstructure increases with the decrease in the thermal fluctuation. This behavior is common to the Y- or Er-substituted compounds, which clarifies that the Fe charge order is not sensitive to the site disorder existing in the Lu layers.

One noticeable feature in the neutron powder-diffraction patterns is the asymmetric and rippling line shape of the superstructure peak. This kind of line shape in neutron diffraction was studied in detail by Zhang *et al.*[18] about two decades ago. According to the reference, the asymmetric line shape with rippling in neutron-diffraction pattern is a result of a two-dimensional (2D) magnetic order in a sample system with coupled bilayers. They also provided a formula for the magnetic scattering intensity as follows. For the coupled-bilayer two-dimensional magnetic powder diffraction, the intensity for the (h,k) Bragg reflection is given by

$$I_{hk} \sim \frac{|F_M|^2}{\sin\theta} F(\theta),$$

where

$$F(\theta) = \int_0^{\pi/2} \exp\left[-\frac{4\pi L^2}{\lambda^2}(\sin\theta\cos\phi - \sin\theta_{hk})^2\right] \times \left|1 + C\exp\left[\frac{i4\pi d}{\lambda}\sin\theta\sin\phi\right]\right|^2 d\phi.$$

Here, θ is the scattering angle, F_M is the magnetic structure factor for the 2D magnetic unit cell, L is a parameter that measures a domain size, θ_{hk} is the Bragg angle for the (hk) reflection, $\lambda = 2\sin\theta_{hk}/[(h/a)^2+(k/b)^2]^{1/2}$, where a and b are 2D unit-cell constants, d is the perpendicular component of the vector connecting the two layers, and C is a constant indicating the two-bilayer coupling types: $C=1$ for ferromagnetic coupling and $C=-1$ for antiferromagnetic coupling. Practically, the coupling constant C can be regarded as a continuous parameter in the range of $[-1,+1]$ for fractional ferromagnetic or antiferromagnetic domains. Figure 3(b) shows our fitting results for the line shape of the $(1/3\ 1/3\ l)$ superstructure peak based on the above diffraction theory. In this analysis, three physical parameters can be evaluated, namely, the coupling constant C, domain size L, and the magnetic interplane distance d. These parameters at 20 K are $C=0.15\pm0.05$, $L=250\pm50$ Å, and $d=50\pm1$ Å for $LuFe_2O_4$, $C=0.10\pm0.05$, $L=200\pm50$ Å, and $d=34\pm1$ Å for $Lu_{0.5}Y_{0.5}Fe_2O_4$, and $C=0.15\pm0.05$, $L=200\pm50$ Å, and $d=35\pm1$ Å for $Lu_{0.5}Er_{0.5}Fe_2O_4$, respectively. The results imply that all the samples have a long-range (~200 Å) magnetic ordering in Fe bilayers and that the bilayers ferromagnetically order, though not perfect, with a period of four- or six-bilayer thickness. To summarize the neutron-diffraction study, Y- or Er-substituted $LuFe_2O_4$ shows very similar behaviors to the mother compound in Fe-valence ordering, magnetic domain size, and magnetic bilayer coupling.

C. XAS and XMCD study

The Fe-valence states of the mother compound, $LuFe_2O_4$, have been examined by various experimental probes such as Fe $2p$ XAS, O $1s$ XAS, and Mössbauer spectroscopy.[10,19] In the charge ordered state below ~330 K, Fe^{2+} and Fe^{3+} ions exist with 1:1 ratio. This feature lasts in the Y- or Er-substituted systems as shown in Fig. 4(a). The Fe $2p$ XAS spectra of $Lu_{1-x}L_xFe_2O_4$ (L=Y and Er; x=0.1 and 0.5) show the two spin orbit split L_3 and L_2 absorption structures. In the L_3 structure, the white lines of Fe^{2+} and Fe^{3+} are clearly resolved as designated by the arrows. The XAS spectra of the L-substituted samples do not show any significant change in weight and shape, which implies the Er or Y substitution does not affect the Fe-valence values. This is also consistent with the superstructure peak observed in the neutron powder-diffraction patterns of the L-substituted samples.

Contrary to the similarity of the XAS spectra, the XMCD spectra reveal a significant change as Y or Er is substituted for Lu in $LuFe_2O_4$ as shown in Fig. 4(b). The dichroism signal ($\Delta\rho$) is a difference between two XAS spectra for different magnetization directions (ρ_+ and ρ_-). In the $\rho_+(\rho_-)$ mode, the photon k vector is parallel (antiparallel) to the sample magnetization direction. The negative sign of the di-

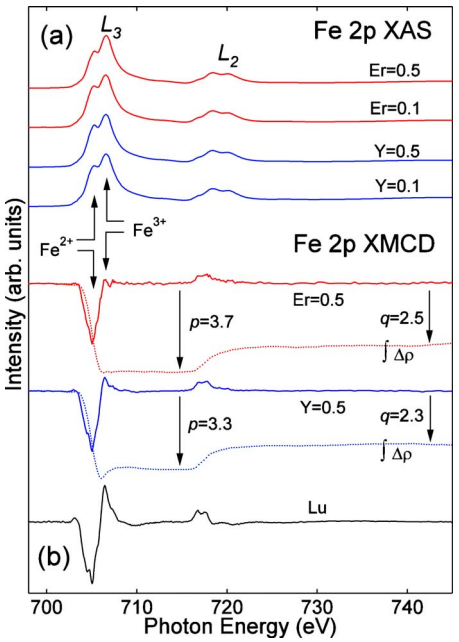

FIG. 4. (Color online) (a) Fe $2p$ XAS spectra of $Lu_{1-x}L_xFe_2O_4$ (L=Y and Er) at 200 K. (b) Fe $2p$ XMCD spectra and its integrations. In the $LuFe_2O_4$ case, the spectrum was obtained from Ref. 10.

chroism in the L_3 edge means that the spin moment direction is parallel to the external magnetic field, and the positive sign in the L_3 edge means that the spin moment direction is antiparallel. Thus, the XMCD spectrum of $LuFe_2O_4$ shows that the net spin moment of $Fe^{2+}(S=2)$ ions is parallel to the applied magnetic field but is antiparallel to that of $Fe^{3+}(S=5/2)$ ions. The smaller dichroism spectral weight at the Fe^{3+} white line than that of Fe^{2+} indicates that not all the spin moments of Fe^{3+} ions are aligned in parallel with each other. These results, combined with the neutron-scattering experiments, gave a specific spin configuration for the ferrimagnetic $LuFe_2O_4$.[10] In Fig. 5, the most probable spin configuration is presented in charge ordered $LuFe_2O_4$. This spin configuration can be understood in terms of the spin-orbit coupling and the superexchange interaction as follows. According to the electronic structure of the unoccupied Fe $3d$ orbitals probed by the polarization dependent XAS spectra of $LuFe_2O_4$,[10] the $d_{yz/zx}$ $[\frac{i}{\sqrt{2}}(|m_l=1\rangle+|-1\rangle)/\frac{-1}{\sqrt{2}}(|1\rangle-|-1\rangle)]$ orbitals have the lowest energy level. This means that the sixth electron in the $Fe^{2+}(3d^6)$ ions occupies the degenerate $d_{yz/zx}$ orbitals with down spin. However, the spin-orbit coupling splits the $d_{yz/zx}$ doublet into $m_l=1$ and -1 states, and the sixth electron occupies $m_l=1$ state more than $m_l=-1$ state. Then, this makes the unquenched orbital moment parallel to the spin moment in Fe^{2+} ions. Meanwhile, the $Fe^{3+}(3d^5)$ ions do not have the unquenched orbital moment because the five electrons half-fully occupy the $3d$ orbitals with up spin. Thus, the next dominant interaction would be the superexchange between the Fe^{3+} ions through the oxygen anions. In Fe_2O_4 bilayers, two kinds of superexchange path exist. One is the path between the Fe^{3+} ions within the Fe^{3+}-rich plane in the charge ordered state as designated by two small red spheres inside rhombus in Fig. 5 and the other is the path between the interlayer Fe^{3+} ions. However, the latter is very small since the angle of Fe^{3+}-O-Fe^{3+}, which is the supplementary angle of β in Fig. 1(b), is around 95°. As a result, the spins of the in-plane Fe^{3+} ions favor the antiparallel alignment as shown in Fig. 5.

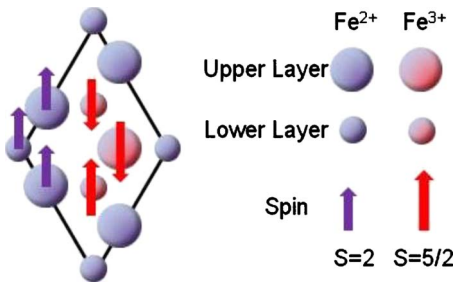

FIG. 5. (Color online) A possible spin configuration in $(Lu,L)Fe_2O_4$ superlattice.

As Y or Er ions are substituted for Lu ions, the XMCD signal of Fe^{3+} ions becomes smaller and disappear but the XMCD signal of Fe^{2+} ions stays almost the same. This contrasting behavior indicates two things about the magnetic interactions of Fe ions in $(Lu,L)Fe_2O_4$. One is that the interaction between the Fe^{2+} ions does not change much with the L concentration and the other is that the alignment of the Fe^{3+} ions changes significantly. The invariance of the magnetic interactions of the Fe^{2+} ions is plausible since only the Fe^{2+} ions have the unquenched orbital moment due to the spin-orbit coupling. Indeed, Y or Er substitution does not affect on the Fe-valence states as is observed in our neutron-diffraction patterns and in Fe $2p$ x-ray absorption spectra. Further, the sum-rule analysis of the XMCD spectra shows that the variation compounds also have a large unquenched orbital moment. Using the sum rule, the ratio of orbital moment (m_o) to spin moment (m_s) can be obtained from the XMCD spectrum and its integration spectrum.[20] With the values of p and q measured in Fig. 4(b), the ratio (m_o/m_s) is estimated to be 0.28 for both Y- and Er-substituted samples. Although this ratio is a little bit smaller than that of $LuFe_2O_4$ ($m_o/m_s=0.34$), it is still quite a large value compared with conventional magnetic oxides. Note that this ratio does not depend on the total magnetization strength of the samples unless the system undergoes a spin phase transition with the increase in the applied magnetic field. Also, note that the periodicity change in the magnetic order along the c direction estimated in the neutron-diffraction study does not affect the analysis of the XMCD spectra.

On the other hand, the disappearance of the dichroism signal at Fe^{3+} edge indicates that the magnetization from the Fe^{3+} ions becomes negligible. Either a perfect antiferromagnetic alignment or losing long-range order by frustration could be possible reasons. However, since the Fe^{3+} ions form a triangular bilayer, a perfect antiferromagnetic ordering is not allowed, so frustration is the most plausible for the reason. The structural distortion with the L substitution also supports this scenario. As is described in the structure analysis section, the substitution affects on the crystal structure of the compounds, making the bipyramidal FeO_5 cages distorted. Through the distortion, the bonding length of Fe-O_{inp} increases and the angle of Fe^{3+}-O_{inp}-Fe^{3+}, which is equiva-

lent to the angle α in Fig. 1(b), decreases. Both of these changes weaken the superexchange interaction between nearest two Fe^{3+} ions in the Fe^{3+}-rich planes. Meanwhile, the decrease in Fe-O_{z1} bonding length, which is the intrabilayer distance, and the increase in the supplementary angle of β enhance the superexchange of the interplane Fe^{3+} ions. As a result, the system may lose a dominant interaction mechanism for the Fe^{3+} spin alignment and be frustrated, giving weak XMCD signal at the Fe^{3+} absorption edge.

IV. SUMMARY

In summary, we substituted Y and Er for Lu in hexagonal bilayered $LuFe_2O_4$ and investigated the crystal structure changes by using neutron powder diffraction. The Rietveld structure analysis revealed that as the substitution increases the crystal unit cell is flattened and the bipyramidal FeO_5 is asymmetrically distorted. The temperature-dependent neutron powder-diffraction patterns showed that the Y- or Er-substituted compounds also have $\sqrt{3}\times\sqrt{3}$ superlattices below ~250 K and that the bilayers ferromagnetically order with a period of four- or six-bilayer thickness. The Fe $2p$ x-ray absorption spectra confirmed that the Y or Er substitution does not affect on the Fe-valence states but x-ray magnetic circular dichroism spectra revealed that the spins of the Fe^{3+} ions become frustrated as the substitution increases. This frustration can be consistently explained by the structure distortion observed in the neutron-diffraction patterns when we consider the weakening of the superexchange interaction between nearest two Fe^{3+} ions in the Fe^{3+}-rich planes of the charge ordered phase.

ACKNOWLEDGMENTS

This work was supported by the Korea Science and Engineering Foundation (KOSEF) grant funded by the Korea government (MEST) (Grant No. 2007-00758), and also partially supported by Nuclear Research & Development Program through the National Research Foundation grant funded by the MEST (Grant No. 2009-0072143). The work at GIST was supported by the KOSEF NCRC program, funded by the MEST (Grant No. R15-2008-006-01002-0).

*ffnhj@chonnam.ac.kr

[1] D. I. Khomskii, J. Magn. Magn. Mater. **306**, 1 (2006).
[2] S.-W. Cheong and M. Mostovoy, Nature Mater. **6**, 13 (2007).
[3] J. van den Brink and D. I. Khomskii, J. Phys.: Condens. Matter **20**, 434217 (2008).
[4] N. Ikeda, H. Ohsumi, K. Ohwada, K. Ishii, T. Inami, K. Kakurai, Y. Murakami, K. Yoshii, S. Mori, Y. Horibe, and H. Kotô, Nature (London) **436**, 1136 (2005).
[5] J. Iida, M. Tanaka, Y. Nakagawa, S. Funahashi, N. Kimizuka, and S. Takekawa, J. Phys. Soc. Jpn. **62**, 1723 (1993).
[6] W. Wu, V. Kiryukhin, H.-J. Noh, K.-T. Ko, J.-H. Park, W. Ratcliff, P. A. Sharma, N. Harrison, Y. J. Choi, Y. Horibe, S. Lee, S. Park, H. T. Yi, C. L. Zhang, and S.-W. Cheong, Phys. Rev. Lett. **101**, 137203 (2008).
[7] M. A. Subramanian, T. He, J. Chen, N. S. Rogado, T. G. Calvarese, and A. W. Sleight, Adv. Mater. **18**, 1737 (2006).
[8] X. S. Xu, M. Angst, T. V. Brinzari, R. P. Hermann, J. L. Musfeldt, A. D. Christianson, D. Mandrus, B. C. Sales, S. McGill, J.-W. Kim, and Z. Islam, Phys. Rev. Lett. **101**, 227602 (2008).
[9] S. Park, Y. Horibe, Y. J. Choi, C. L. Zhang, S.-W. Cheong, and W. Wu, Phys. Rev. B **79**, 180401(R) (2009).
[10] K. T. Ko, H.-J. Noh, J.-Y. Kim, B.-G. Park, J.-H. Park, A. Tanaka, S. B. Kim, C. L. Zhang, and S.-W. Cheong, Phys. Rev. Lett. **103**, 207202 (2009).
[11] T. Roisnel and J. Rodriguez-Carvajal, FULLPROF, 2000.
[12] M. Isobe, N. Kimizuka, J. Iida, and S. Takekawa, Acta Crystallogr., Sect. C: Cryst. Struct. Commun. **46**, 1917 (1990).
[13] Y. Yamada, S. Nohdo, and N. Ikeda, J. Phys. Soc. Jpn. **66**, 3733 (1997).
[14] N. Ikeda, S. Nohdo, and Y. Yamada, J. Korean Phys. Soc. **32**, S165 (1998).
[15] Y. Yamada, K. Kitsuda, S. Nohdo, and N. Ikeda, Phys. Rev. B **62**, 12167 (2000).
[16] Y. Zhang, H. X. Yang, C. Ma, H. F. Tian, and J. Q. Li, Phys. Rev. Lett. **98**, 247602 (2007).
[17] A. D. Christianson, M. D. Lumsden, M. Angst, Z. Yamani, W. Tian, R. Jin, E. A. Payzant, S. E. Nagler, B. C. Sales, and D. Mandrus, Phys. Rev. Lett. **100**, 107601 (2008).
[18] H. Zhang, J. W. Lynn, and D. E. Morris, Phys. Rev. B **45**, 10022 (1992).
[19] B. K. Bang, S. B. Kim, S.-W. Cheong, and C. S. Kim, Phys. Status Solidi B **244**, 4566 (2007).
[20] C. T. Chen, Y. U. Idzerda, H.-J. Lin, N. V. Smith, G. Meigs, E. Chaban, G. H. Ho, E. Pellegrin, and F. Sette, Phys. Rev. Lett. **75**, 152 (1995).